Experimental investigation of activated carbon prepared from apricot stones material (ASM) adsorbent for removal of malachite green (MG) from aqueous solution

Moussa Abbas [ID]

Laboratory of Soft Technologies and Biodiversity, Faculty of Sciences, University M'hamed Bougara, Boumerdes, Algeria

Abstract

The adsorption of malachite green onto activated carbon prepared from apricot stones material has been investigated at batch conditions. The effects of contact time (0–60 min), initial pH (3–11), agitation speed (100–700 r/min), temperature (298–343 K), adsorbent dose (1–10 g/L), and malachite green concentration (4.45–17.6 mg/L) on the malachite green adsorption by apricot stones material have been studied. Malachite green removal increases over the contact time until equilibrium. The batch adsorption experiments were carried out to optimize the physical parameters on the malachite green removal efficiency. It has been found that 23.80 mg/g at 25°C and 88.05 mg/g at 70°C were removed. The kinetic parameters, rate constants and equilibrium adsorption capacities, were calculated and discussed for each kinetic model. The adsorption of malachite green onto apricot stones material is well described by the pseudo second-order equation. The experimental isotherm data were analyzed by different models; the adsorption follows the Langmuir model, providing a better fit of the equilibrium data. The thermodynamics parameters such as the negative free energy $\Delta G°$ (-0.191 to -4.447 kJ/mol) and positive enthalpy $\Delta H°$ (50.86 kJ/mol) indicated the spontaneous and endothermic nature of the malachite green adsorption with a chemisorption process.

Corresponding author:
Moussa Abbas, Laboratory of Soft Technologies and Biodiversity, Faculty of Sciences, University M'hamed Bougara, Boumerdes 35000, Algeria.
Email: moussaiap@gmail.com

Introduction

The effluents from the textile, leather, food processing, dyeing, cosmetics, paper, and dye manufacturing industries are the main sources of the aquatic pollution (Abbas and Trari, 2015). Colored wastewaters are a direct result of the production of dyes. Indeed, many dyes and their degradation products are highly toxic for living organisms particularly the malachite green (MG; Kannan and Sundaram, 2001). Therefore, the discoloration of dyes' effluents is an important aspect for the water treatment prior to release to the aquatic environment. The dyes are not easily degradable and are difficult to remove from wastewater by the conventional techniques (Isık and Sponza, 2005). The presence of dyes in water gives rise to a chemical and biochemical oxygen demands and high-suspended solids. Considering the discharged volume and effluent combustion, the wastewater from the textile industry (Iqbal and Ashiq, 2007) is considered as one of the most polluting among all industrial sectors. Their presence, even at very low concentrations, is visible and consequently undesirable; it may dramatically affect the photosynthetic activity in the aquatic life due to the reduced light penetration. Nowadays, various physicochemical techniques have been studied to assess their applicabilities for the treatment of this type of effluents. Among the known processes, one can include the coagulation, ozonation, precipitation, flocculation, and adsorption (Abbas et al., 2019). The latter is an effective method due to its low maintenance, simple operation, and removal effectiveness (Leigen et al., 2019). Moreover, it provides an attractive alternative, especially if the adsorbent is low cost and readily available. In this respect, activated carbon is a versatile material for the adsorption process, but remains relatively expensive. Consequently, many works were concentrated on the feasibility of abundantly available substances for the synthesis of activated carbon (Qi-Xia et al., 2019). This has prompted a growing research in the production of activated carbons from renewable and cheaper precursors which are mainly industrial and agricultural by-products, for the water treatment. Indeed, the commercial activated carbons remain relatively expensive, and their production and regeneration cost are limiting factors. As a result, much research has focused on low-cost precursors, especially from agricultural wastes such as rubber seed coat (Rengaraj et al., 2002), olive stones (El-Sheikh et al., 2004), sawdust (Malik et al., 2007), coir pith (Namasivayam and Kavitha, 2002), bamboo (Hameed et al., 2007), and apricot stones (Abbas et al., 2016).AQ1 The remarkable adsorption capacity of activated carbons is due to their well-developed porous structure and pore size distribution, as well as the surface functional groups. The adsorption efficiency depends on the pH, polarity, solubility, molecular size of adsorbate, and the presence of other ions in solution. However, the specific mechanism by which the adsorption of organic compounds takes place on active carbons is not yet fully known. Agricultural by-products exist in large amounts and about 256,890 tons of apricot stones are produced annually in Algeria (Food and Agriculture Organization of the United Nations (FAO), 2017, Table 1). In the past, these by-products were used as fuel in rural areas but now the preparation of activated carbon is considerably encouraged and apricot stone constitutes a cheap precursor for activated carbon source. Therefore, it is important to evaluate its performance as adsorbent (Abbas et al., 2014). The advantage of using an abundant and available residual biomass namely the apricot stone, as a raw material for activated carbons gives an economical interest to the technical studies. The apricot stone used in the present study was prepared by both physical and chemical activations and this study was performed with the aim to optimize the initial dye concentration, pH, grain size, contact time, adsorbent dose,

Table 1. The state of apricot culture (FAO, 2017).

Countries	Production (tones)
Turkey	985,000
Uzbekistan	532,562
Italy	266,372
Algeria	*256,890*
Iran	239,712
Pakistan	178,957
Spain	162,872
France	148,500
Afghanistan	131,816
Moroco	112,538

Table 2. Chemical and physical properties of basic dye, malachite green.

Chemical properties	
Brute formula	$C_{23}H_{25}ClN_2$
Molecular weight	364.911 ± 0.023 g/mol
Composition (%)	C: 75.0, N: 7.68
	Cl: 9.72, H: 6.91
Wavenumber (λ_{max})	614 nm
Name	CI 42000, Basic Green, malachite green
pKa_1	1.3
pKa_2	12.8

agitation speed, and temperature. In addition, the equilibrium adsorption data were fitted to different models to get constants related to the adsorption process. Equilibrium and kinetic analysis were performed to determine the parameters governing the adsorption rate, the optimization of physical parameters in the MG elimination, and the possibility of using this material as an inexpensive adsorbent for dye removal.

Experimental

Materials and methods

Analytical grade reagents were used in all experiments. MG (99%) a basic dye was purchased from Merck Company; its chemical and physical properties are listed in Table 2. Activated carbon was elaborated by carbonization and chemical activation with H_3PO_4 (85%) as follows:

Chemical activation. The apricot kernels from Boumerdes region (30 km east of Algiers) are air-dried, ground, and screened to obtain two fractions with average sizes ranging from 63 μm to 2.5 mm.

100 grams of the selected fraction of the precursor were impregnated in H_3PO_4 solution of purity (85%) in a mass ratio (1/2), for 24 h to allow a good contact between acid and

apricot nucleus shell and to increase the pores' diameter. The material was thoroughly washed in distilled water to remove free acid until the pH reaches 6.8 and dried at 105°C. Then, the power was introduced into a programmable muffle furnace at 250°C for a period of 4 h.

The apricot stones were mechanically ground and screened to powders of different particle sizes: <63, 63–80, 80–100, 100–200, 200–315, 315–800 μm and 0.8–1, 1–1.6, 1.6–2 mm.

The temperature, time, and phosphoric acid were selected according to the recent literature, economic cost of preparation, and environmental impact.

Characterization of activated carbon

Chemical and physical analysis of the prepared activated carbon (ASM). The Fourier transform infrared spectroscopy (FTIR) was used to identify the characteristic functional groups of ASM; 5 mg of ASM were mixed with KBr of spectroscopy quality and pressed under a pressure of 4500 lbf/in^2 to form thin disc. The spectra were plotted with a Perkin Elmer 2000 infrared spectrometer. The sample was scanned from 4000 to 400 cm^{-1} for 16 times to increase the signal-to-noise ratio.

To visualize the surface structure of the prepared ASM before MG adsorption, scanning electron micrographs were taken with different resolutions thanks to a scanning electron microscope (JOEL-5910) under the following operating conditions: (Quanta, WD, HFW) 50, 9.3, 128 μm, respectively, detector: LFD, spot: 4.0, HV: 5.00 kV, magnification: 2000×.

The specific surface areas of adsorbents were measured from the N_2 adsorption–desorption isotherm using a pore size Micrometric-9320 equipment surface analyzer at the relative pressure ($P/P_o = 0.308$). The micropore volumes were evaluated with the accumulative pore volume using the t-plot method. The total pore volume was calculated from the volumes of N_2 absorbed at relative pressure ($P/P_o = 0.349$).

For the elemental analysis, the sample (∼2 mg) was finely ground and placed in a microanalyzer (type LECO CHNO-932) equipped with an electronic balance and a programmable temperature regulator.

The carbon, hydrogen, and nitrogen contents were determined and the oxygen content was deduced after complete combustion of the sample. Nevertheless, for most organic and mineral compounds, carbon predominates while nitrogen is at a low level.

The chemical composition of ASM in the form of oxides was determined by X-ray fluorescence (XRF) in a Rigaku RIX-3000 equipment under the following operating conditions: stingray: $K_{L\alpha}$, analyzer crystal: LiF200, collimator: 150 μm, sensor: flow, Not: 0.08 degrees, V: 0.16 s/step, I: 125 mA and V: 60 kV.

The prepared activated carbon was characterized by physical methods (bulk density and surface area) as well as chemical and adsorption properties (point of zero charge: pHpzc).

The conductivity was measured with a conductimeter type Erwika. pHpzc of ASM was obtained by the Cerovich method using 20 mL of KNO_3 solutions (0.01 M) placed in closed conical flasks. The pH of each solution was adjusted in the range (2–14) by addition of HCl or NaOH (0.1 M). Thereafter, 0.1 g of ASM was added and the final pH was measured after 24 h under agitation; pHpzc corresponds to the intersection final pH = initial pH.

Batch mode adsorption studies. The effects of the experimental parameters namely the initial MG concentration (4.45–17.6 mg/L), pH (3–11), adsorbent dose (1–10 g/L), agitation speed (100–700 r/min), and temperature (298–343 K) on the MG elimination were studied in batch

configuration for variable contact times (0–60 min). The stock solutions were prepared by dissolving the accurate amount of MG (99%) in distilled water, and diluted to different concentrations; pH was adjusted with HCl or NaOH (0.1 M). For the kinetic studies, ASM were contacted with 10 mL of MG solutions in Erlenmeyer flasks and placed on a rotary shaker (300 r/min); the samples were withdrawn regularly and centrifuged (3000 r/min, 10 min). The residual MG concentration in the supernatant was analyzed with a Perkin Elmer UV-visible spectrophotometer model 550S ($\lambda_{max} = 494$ nm). The amount (q_t) of MG ions (mg/g) adsorbed by ASM was calculated from the relation

$$q_t = \frac{(C_0 - C_e) \cdot V}{m} \tag{1}$$

where C_o is the initial MG concentration (mg/L), C_t the concentration at time (t), V the volume of solution (L), and m the ASM mass (g).

Error analysis: Due to the inherent bias resulting from the linearization of the isotherm models, the non-linear regression root mean square error (RMSE), the sum of error squares (SSE), and chi-squares (X^2) tests were used as criteria for the quality of fitting (Zahia et al., 2019a)

$$\text{RMSE} = \sqrt{\frac{1}{N-2} \cdot \sum_{1}^{N} (q_{e,exp} - q_{e,cal})^2} \tag{2}$$

$$\text{SSE} = \frac{1}{N} \sum_{n=1}^{\infty} (q_{e,cal} - q_{e,exp})^2 \tag{3}$$

$$X^2 = \sum_{1}^{N} \frac{(q_{e,exp} - q_{e,cal})^2}{q_{e,cal}} \tag{4}$$

where $q_{e(exp)}$ (mg/g) is the experimental uptake, $q_{e(cal)}$ the calculated uptake using a model (mg/g), and N the number of experimental observations (the number of data points); the smaller RMSE value indicates the better fitting.

Results and discussion

Characterization of the prepared ASM

The physical and chemical properties of ASM and the elementary analysis are gathered in Table 3. Examination of the physico-chemical properties of the elaborate ASM (Figure 1) shows that the chemical and physical activation has developed a porosity and increased the specific surface area up to 80.05 m^2/g for the fixing the maximum pollutant. The elemental analysis shows the predominance of the percentage of carbon (48.45%); in correlation with the adsorbents reported in the literature. The analysis by laser heating shows that the precursor used has a low moisture content (1.48%), the percentage of organic matter determined by XRF is found to be 98.32%.

Table 3. Physical and chemical properties of the apricot stones activated carbon (ASM).

Elemental analysis (%)	C: 48.45	H: 6.03	N: 0.44	O: 45.08
pH_{zpc}	7.06			
Surface area (m^2/g)	88.05			
Average pore diameter (Å)	176.3			
Average pore volume (mL/g)	0.264			
Conductivity (μS/cm)	112			
Humidity (%)	1.48			
The rate of ash (%)	1.68			
The percentage of organic matter (%)	98.32			
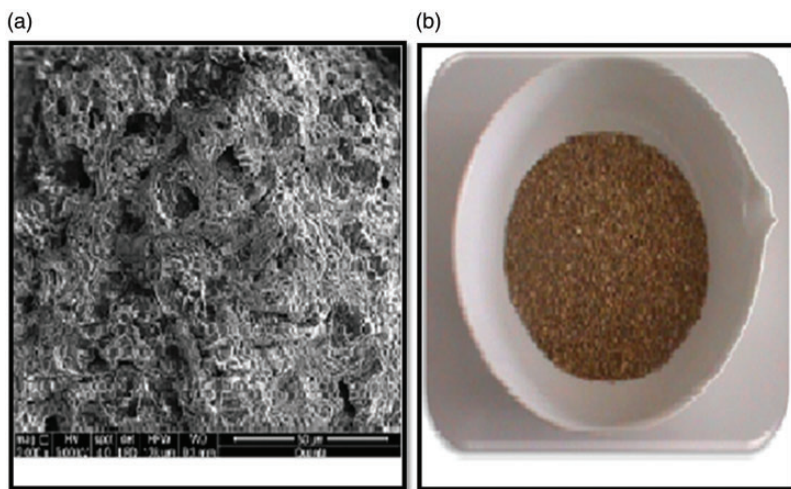
Figure 1. Activated and natural apricot stone.

Structural characterization by infrared spectroscopy

The FTIR spectra of the adsorbent (Figure 2) show many absorption peaks, characteristic of functional groups of the adsorbent (Abbas et al., 2018). The large band in the region (3122–$3680\,cm^{-1}$) is due to –OH groups (unrelated –OH function and intermolecular hydrogen band). The bands centered at 2929 and $1508\,cm^{-1}$ suggest the presence of –CH_2 groups (symmetric and antisymetric) while the band in the region (1600–$1665\,cm^{-1}$) indicates the presence of C–H, –C=C– and C=C groups. The peak at $1732\,cm^{-1}$ is assigned to C=O bond in the carboxylic groups. Such results clearly show that the functional groups including carboxylic and hydroxyl groups contribute to the MG adsorption.

To explain the adsorption process that took place between the pollutant and the adsorbent charged with the opposite sign, attractive electrostatic forces are exerted between the charges for fixing in the surface sites which gradually decrease over the dye occupation. Once the saturation is reached, the pollutant enters the deepest sites under the effect of the
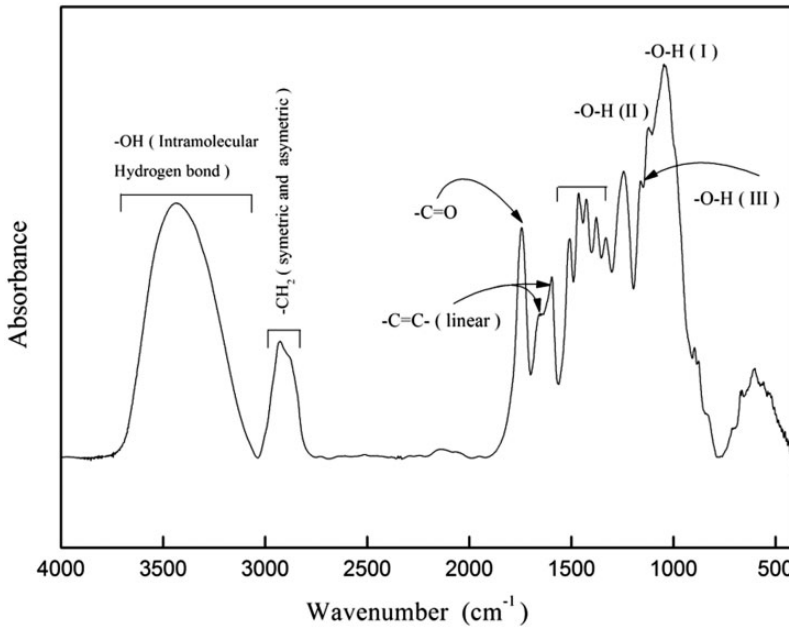
Figure 2. Spectrum of FTIR analysis from apricot stone.

gradient concentrations; the general mechanism can be summarized by the following sequence of reactions:

- Transfer of the pollutant from the outer to inner layer (very fast step).
- Displacement of the pollutant until it comes into contact with the adsorbent (rapid step).
- Diffusion of the pollutant into the adsorbent under a concentration gradient (slow step).
- Adsorption of the pollutant in the micropores (very fast step).

Adsorption mechanism

The adsorption mechanism can be explained as a function of the interactions of functional groups of the adsorbent with the dye. For this, the second-order kinetic model is in perfect correlation with the experimental results. Intraparticular diffusion does not dominate the mechanism but contributes to the adsorption process. The free energy and enthalpy change during the adsorption of MG on ASM, suggesting that chemisorption (the formation of new chemical bonds), are the main mechanisms controlling the adsorption process. According to Iqbal and Ashiq (2007), the presence of larger pores promotes higher adsorption capacities, particularly for dyes. The surface chemistry is another important factor that controls the adsorption. Highly functionalized surfaces with carboxylate and ketone groups can readily chemisorb cationic dyes.

The carbonaceous material has the potential to absorb the MG; the considerable number of oxygen-containing functional groups on the surface of the carbonized adsorbent provides adequate adsorption sites and increases the adsorption capacity of the pollutant. The adsorption mechanisms are mainly due to the formation of hydrogen bonds, hydrophobic interactions, and electrostatic forces of the pollutants with the activated carbon

surface. The main binding sites of MG by activated carbons are the hydroxyl and carboxyl groups on the surface of the ASM adsorbent that react with polar molecules and various functional groups. The surface of the porous activated carbon may include electrically charged groups (pHzpc). The isoelectric pH of ASM determined by the Cerovich method is 7.05, this is explained by: a predominance of negative adsorbent charges for above 7.05, favorable for the fixation of MG, a cationic dye, because the electrostatic forces are attractive for the formation of new bonds, which is correlated with the results obtained according to the thermodynamic study (chemisorption process). A predominance of the adsorbent positive charges below pH 7.05 makes the attraction of the MG pollutant overcome, since there is repulsion between the positive charges of the pollutant and the positive charges of the adsorbent. This phenomenon causes a low dye adsorption (only by force of hydrogen bonds of London, Kessan). This observation was reworked during the study of the pH effect of pH on the adsorbed quantity of MG (pH < 7.05).

Effect of analytical parameters

In the first stage of batch MG adsorption onto ASM, the effect of grain sizes is examined. Significant variations in the elimination capacity and removal efficiency were observed from 63 μm to 2 mm, showing that the best performance occurs in the range (800 μm to 2 mm). If we examine the effect of granulometry (Figure 3), we notice that for small dimensions 63–80, 80–100, 100–200, 200–315, and 315–800 μm the adsorbed quantity gradually increases from
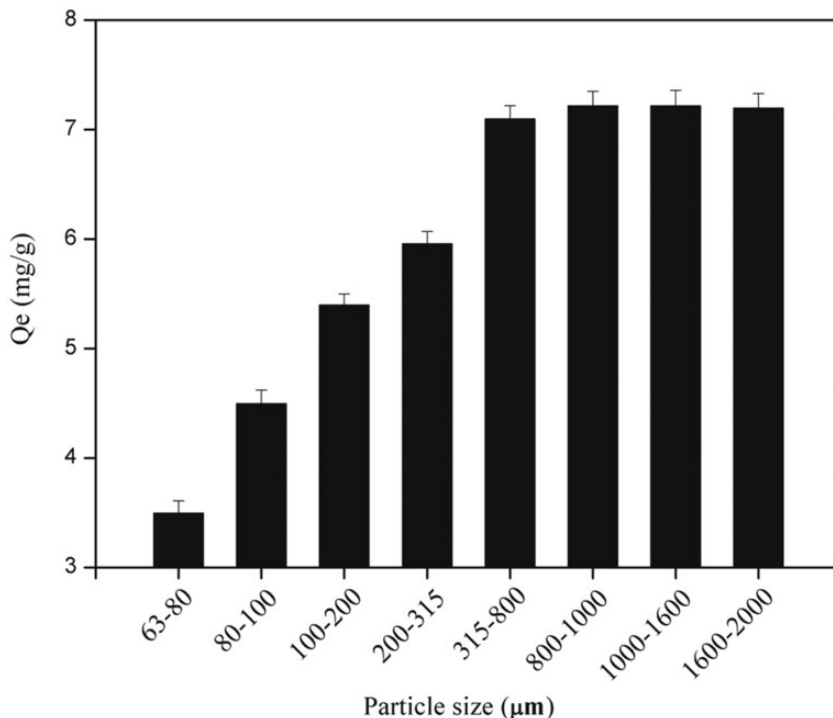
Figure 3. Effect of particle size on the MG adsorption efficiency (*T*: 25°C, C_0: 10 mg/L, *V*: 10 mL, contact time: 40 min, stirring speed: 400 r/min, adsorbent dosage: 1 g/L and pH: 10).

3.5 to 7.3 mg/g. The adsorption is maximal in the region (800 μm–2 mm) which is explained by the saturation of the adsorbent pores for a quantity of 7.5 mg/g. Moreover, this phenomenon can be interpreted by the presence of large adsorbent particles with the presence of larger surface pores (longer and deeper pore length). The electrostatic attraction of the pollutant by the adsorbent sites is favorable, allowing an increase in the uptake dye quantity. The size in the range of 800 μm–2 mm is consequently used in all adsorption experiments.

The pH is a crucial parameter in adsorption and the percentage of MG removal increases consistently with decreasing pH (Figure 4). The pH effect on the MG adsorption by ASM can be explained on the basis of pHpzc, for which the charge of the adsorbent surface is positive below pHpzc of (ASM = 7.05). As the pH decreases, the number of positively charged sites augments and improves the MG adsorption by electrostatic attractions. Similar experimental details have been reported (Abbas et al., 2018).

Figure 5 presents the influence of the stirring speed on the MG adsorption on ASM. The maximum uptake was obtained for variable speeds (400–450 r/min). Such moderate speed gives a good homogeneity for the mixture suspension and precludes the vortex phenomenon.

The adsorption capacity of MG increases over time to reach a maximum after 40 min and thereafter tends to saturation, indicating that no more MG molecules are further removed from the solution. The initial MG concentration from 4.45 to 17.6 mg/L yields an increased adsorbed amount from 3.60 to 8.20 mg/g (Figure 6). This is ascribed to the increased driving force which comes from the concentrations gradient which overcomes the mass transfer resistance of MG ions between the liquid and solid phases.

For the first stage of batch adsorption onto ASM and the influence of adsorbent dose is examined. Significant variations in the uptake capacity and removal efficiency for various
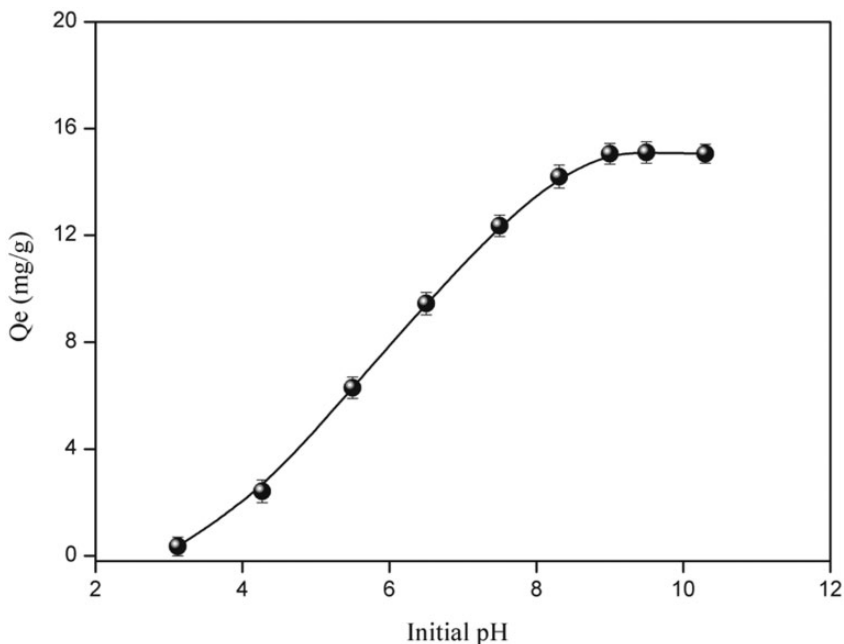
Figure 4. Effect of pH on the MG adsorption efficiency (*T*: 25°C, *C*₀: 10 mg/L, *V*: 10 mL, contact time: 40 min, stirring speed: 400 r/min and adsorbent dosage: 1 g/L and particle size: 800–2000 μm).
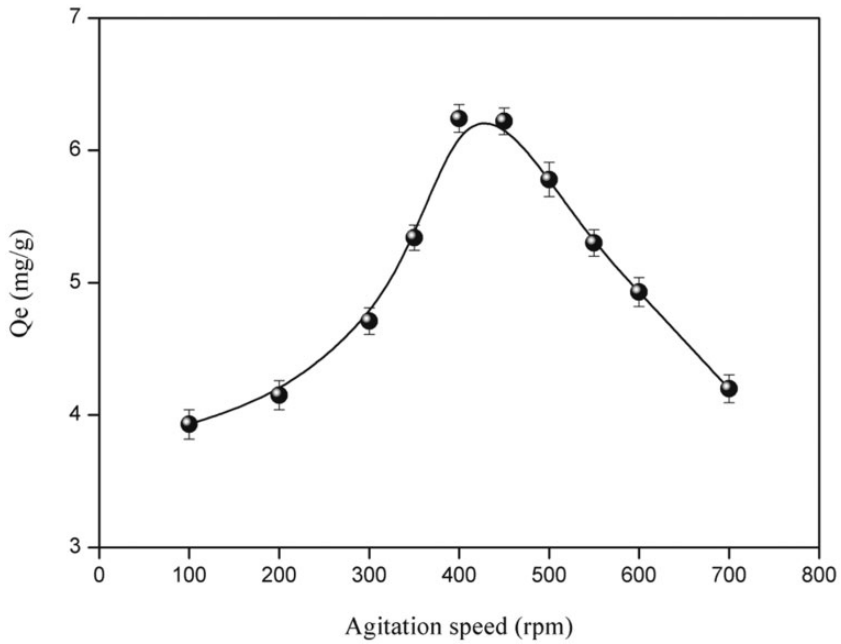
Figure 5. Effect of stirring speed on the MG dye adsorption capacity (*T*: 25°C, C_0: 10 mg/L, pH:10, absorbent dosage: 1 g/L, particle size: 800–2000 μm).
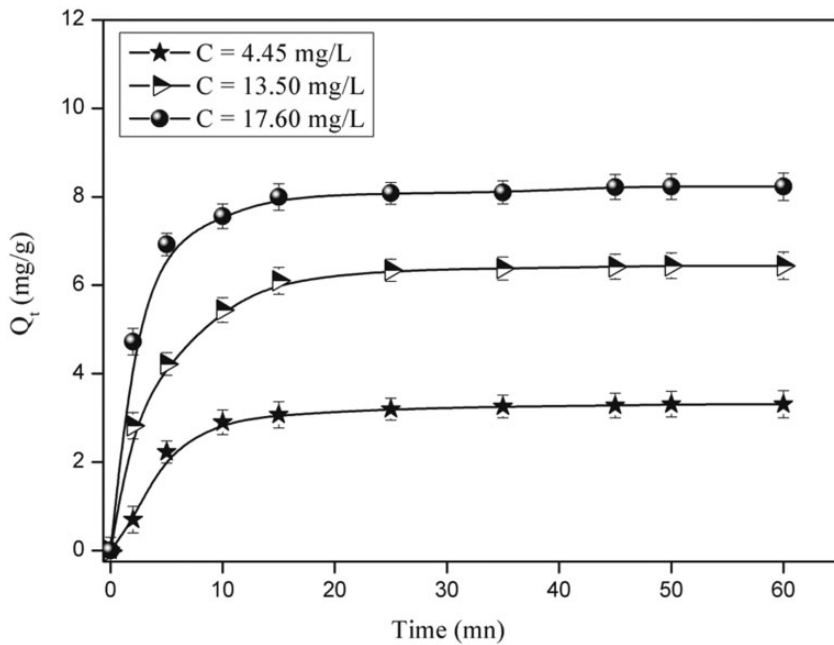
Figure 6. Effect of the contact time on the adsorption of MG onto ASM for different initial concentrations (*T*: 25°C, pH: 10, stirring speed: 400 r/min, absorbent dosage: 1 g/L, and particle size: 800–2000 μm).
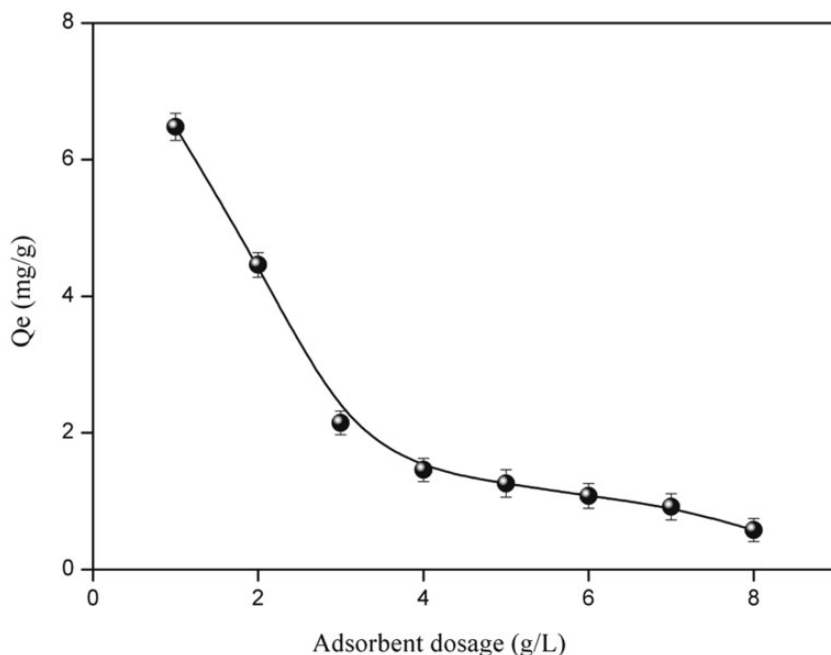
Figure 7. Effect of adsorption dose on the MG dye adsorption capacity (T: 25°C, C_0: 10 mg/L, pH: 8, stirring speed: 400 r/min, contact time: 40 min and particle size: 800–2000 μm).

adsorbent doses (1–10 g/L) indicate that the best performance is obtained for a dose of 1 g/L (Figure 7). This result was expected because the removal efficiency generally increases by the fact that more mass available, more the contact surface offered to the adsorption. Moreover, higher adsorbent dose in solution leads greater availability of exchangeable sites for the ions. The decrease in the dye adsorption with the increase of the adsorbent dose is due to a large amount of adsorption sites on the surface of the adsorbent, which implies that a large amount of adsorbate is required to saturate the adsorbent.

Adsorption isotherms

The shape of the isotherms is an experimental tool to diagnose the type of the adsorption. They are classified in four groups namely L, S, H, and C (Giles et al., 1960), and ASM at (25°C and 70°C) displays L type (Figure 8). The initial part of the L curve indicates a small interaction between the basic dye MG and the carriers at low concentrations. However, as the MG concentration in the liquid phase increases, the adsorption occurs more readily. This behavior is due to a synergistic effect, with the adsorbed MG molecules facilitating the adsorption of additional molecules as a result of attractive interaction adsorbate–adsorbate. The equilibrium isotherm model is used to describe the adsorption data; the underlying thermodynamic parameters of these models provide insights for the adsorption mechanism, surface properties, and affinity of the adsorbent. The importance of obtaining the best isotherm becomes more significant, because as more applications are developed, more accurate and detailed isotherm descriptions are required for the adsorption system designs.
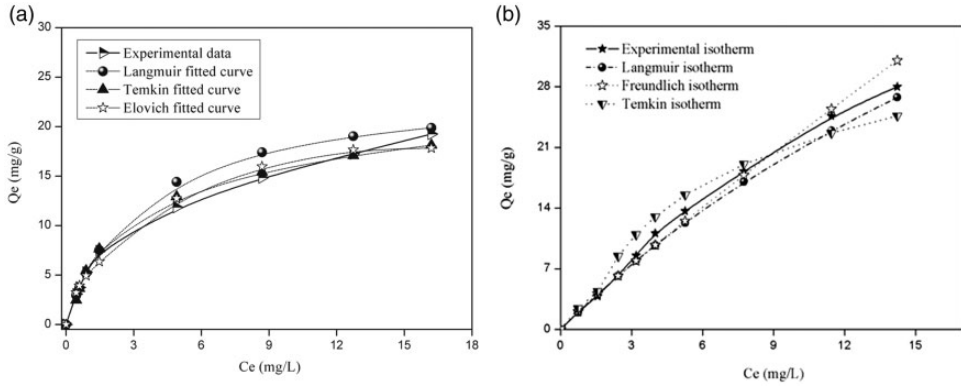
Figure 8. Adsorption isotherm of MG by ASM at temperature a) 25°C and b) 70°C.
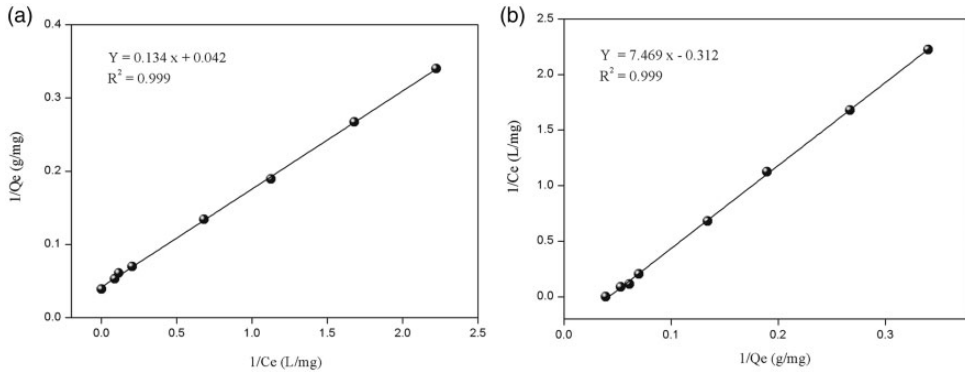
Figure 9. (a) and (b): The Langmuir isotherms modeling at 25°C and 70°C respectively of MG adsorption onto ASM.

The Langmuir model (Gerente et al., 2007) is the best known and most widely applied, it is represented by the linear form

$$\frac{1}{q_e} = \frac{1}{q_{max}} - \frac{1}{q_{max} \cdot K_L \cdot Ce} \tag{5}$$

where C_e is the equilibrium concentration (mg/L), q_{max} the monolayer adsorption capacity (mg/g), and K_L the constant related to the free adsorption energy (L/mg), determined from the plot $(1/q_e)$ versus $(1/C_e)$. The applicability to the adsorption is compared by evaluating the statistic RMSE values at 25°C. The smaller RMSE values obtained for the models indicate a better fitting. The essential features of the Langmuir isotherm (Figure 9(a) and (b)) can be expressed in terms of dimensionless separation factor R_L (Zahia et al., 2019a).

The Freundlich isotherm (Freundlich, 1906) is valid for non ideal adsorption on heterogeneous surfaces as well as multilayer sorption

$$\ln q_e = \ln K_F + \frac{1}{n} \cdot \ln C_e \tag{6}$$

The constant K_F characterizes the adsorption capacity of the adsorbent ($mg^{1-1/n}\ L^{1/n}\ g^{-1}$) while n is an empirical constant related to the magnitude of the adsorption driving force. Therefore, the plot $\ln q_e$ versus $\ln C_e$ permits the determination of both the constant K_F and n.

The Temkin isotherm describes the behavior of adsorption systems on heterogeneous surfaces, and is applied in the following form (Temkin and Pyzhev, 1940)

$$q_e = \frac{RT}{b} \cdot \mathrm{Ln}AC_e = B.\mathrm{Ln}A + B\mathrm{Ln}C_e \tag{7}$$

The adsorption data are analyzed according to equation (7). Therefore, the plot q_e versus $\ln C_e$ leads to determine the constants A and B.

The Elovich isotherm (Ozcan et al., 2006) is based on the principle of the kinetic, assuming that the number of adsorption sites augments exponentially with the adsorption, implying a multilayer adsorption described by

$$\ln \frac{q_e}{C_e} = \ln(q_{max}.K_E) - \frac{q_e}{q_{max}} \tag{8}$$

where K_E (L/mg) is the Elovich constant at equilibrium, q_{max} (mg/g) the maximum adsorption capacity, q_e (mg/g) the adsorption capacity at equilibrium, and C_e (g/L) the concentration of the adsorbate at equilibrium. Both K_E and q_{max} are calculated from the plot of $\ln (q_e/C_e)$ versus q_e.

Redlich-Peterson equation (Limousin et al., 2007). This three-parameter mono soluted model is one of the most used in the literature because it is advertised as applicable over a wide range of concentrations. It is an empirical model combining the parameters of the Langmuir and Freundlich equations and its equation is as follows

$$\frac{q_e}{q_{max}} = \frac{K_1.C_e}{\left(1 + (K_1.C_e)^n\right)} \tag{9}$$

The theoretical parameters along with the determination coefficients RMSE, SSE, and X^2 are listed in Table 4. One can see that the Langmuir isotherm model exhibits the higher RMSE, X^2, and SSE values.

Adsorption kinetics

The kinetic study is important in the adsorption, it describes the uptake rate of adsorbate and controls the residual time of the whole process. The pseudo first-order and pseudo second-order (Figures 10 and 11) are selected in this study to describe the adsorption.

The pseudo first-order equation (Lagergren, 1998) is given by

$$\log(q_e - q_t) = \log q_e - \frac{K_1}{2.303} \cdot t \tag{10}$$

The pseudo second-order model (Ho and Mc Kay, 2000) is expressed by

$$\frac{t}{q_t} = \frac{1}{K_2 \cdot q_e^2} + \frac{1}{q_e} \cdot t \tag{11}$$

**Table 4.** Sorption isotherm coefficients of different models.

Temperature		Parameters	
Model		$T = 25°C$	$T = 70°C$
Langmuir (I)	$1/Q_e = f(1/C_e)$	Q_{max}: 23.80 mg/g K_L: 0.314 L/mg R^2: 0.999 X^2: 0.188 SSE: 0.35 RMSE: 0.59	Q_{max}: 83.33 mg/g K_L: 0.0085 g/mg R^2: 0.999 X^2: 0.208 SSE: 0.39 RMSE: 0.72
Langmuir (V)	$1/C_e = f(1/Q_e)$	Q_{max}: 23.94 mg/g K_L: 0.312 L/mg R^2: 0.999 X^2: 0.185 SSE: 0.37 RMSE: 0.61	Q_{max}: 88.5 mg/g K_L: 0.0088 g/mg R^2: 0.999 X^2: 0.207 SSE: 0.38 RMSE: 0.68
Freundlich	$Ln\ Q_e = f(Ln\ C_e)$	K_F: 2.199 $(mg^{1-1/n}L^{1/n}g^{-1})$ $1/n$: 1.917 R^2: 0.989 X^2: 212.33 SSE: 14787.9 RMSE: 121.61	K_F: 0.922 mg/g $1/n$: 0.845 R^2: 0.996 X^2: 256.33 SSE: 15678.9 RMSE: 128.61
Elovich	$Ln(Q_e/C_e) = f(q_e)$	Q_{max}: 8.62 mg/g K_L: 1.198 g/mg R^2: 0.984 X^2: 0.064 SSE: 0.092 RMSE: 0.303	Q_{max}: 142.8 mg/g K_L: 0.0088 g/mg R^2: 0.89 X^2: 0.123 SSE: 10.125 RMSE: 1.36
Temkin	$Q_e = f(Ln\ C_e)$	K_T: 3.904 L/mg β_T: 4.37 ΔQ: 13.556 kJ/mol β_T: $RTQ_m/\Delta Q$ R^2: 0.987 X^2: 0.055 SSE: 0.036 RMSE: 0.189	K_E: 0.2028 L/mg β_T: 10.028 ΔQ: 25.167 kJ/mol β_T: $RTQ_m/\Delta Q$ R^2: 0.948 X^2: 0.066 SSE: 0.055 RMSE: 2.189
Redlich-Peterson	$C_e/Q_e = f(C_e^n)$	K: −3.904 g/L Q_m: 8.88 mg/g R^2: 0.993 X^2: 1.236 SSE: 10.236 RMSE: 7.125	

RMSE: root mean square error; SSE: sum of error squares.

where q_t (mg/g) is the amount of MG adsorbed at various times t (min), K_1 the rate constant (min^{-1}) and K_2 the rate constant of the pseudo-second order kinetic (g/mg.min). For the pseudo-first order kinetic, the experimental data deviate from linearity as evidenced by the low q_e values and coefficients and is therefore inapplicable for the present system.
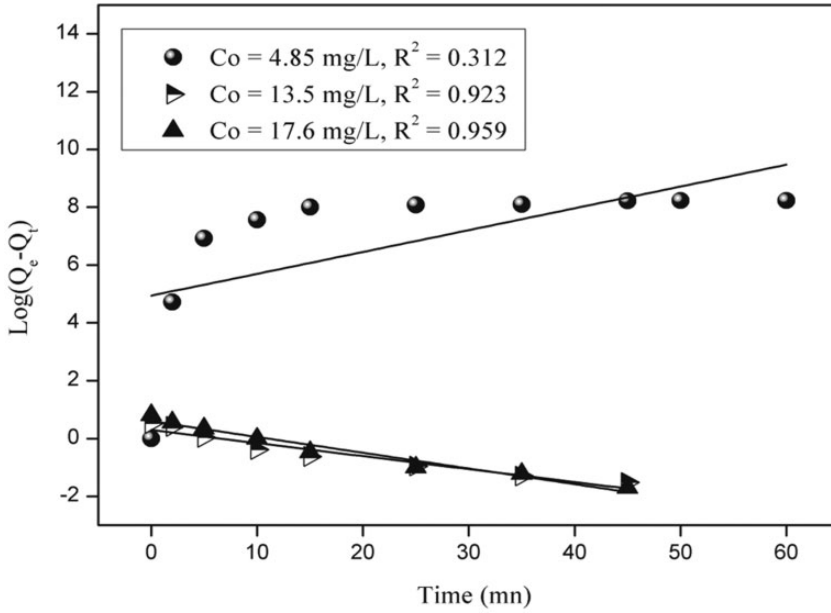
Figure 10. Pseudo first-order kinetic for the adsorption of MG onto ASM (pH: 10, 800–2000 μm particle size, 1 g/L adsorbent dosage, 400 r/min stirring speed, temperature 25°C, and contact time: 40 min).
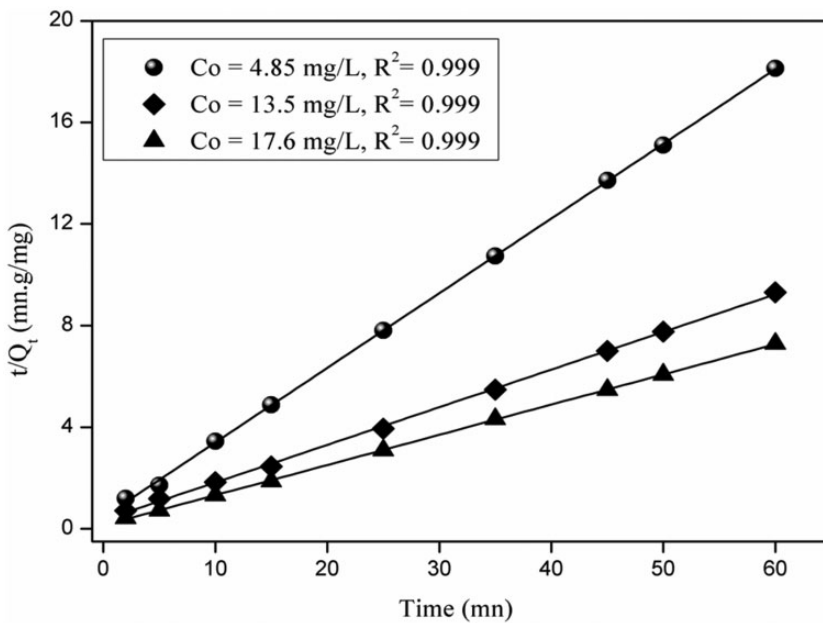
Figure 11. Pseudo-second order kinetic for the adsorption of MG onto ASM (pH: 8, 800–2000 μm particle size, 1 g/L adsorbent dosage, 400 r/min stirring speed, temperature 25°C, and contact time: 40 min).

Table 5. Kinetic parameters for adsorption of MG ions onto ASM.

C_o (mg/L)	2^{ieme} Order					I^{ier} Order			
	Q_{ex} (mg/g)	Q_{cal} (mg/g)	R^2	$\Delta Q/Q$ (%)	K_2 (g/mg.mn)	Q_{cal} (mg/g)	R^2	$\Delta Q/Q$ (%)	K_1 (mn^{-1})
4.45	3.31	3.460	0.999	4.33	0.1218	1.96	0.923	40.78	0.045
13.5	6.44	6.757	0.999	4.69	0.0633	3.97	0.959	38.35	0.054
17.6	8.23	8.40	0.999	2.02	0.1042	3.53	0.889	55.95	0.053

C_o (mg/L)	Elovich		
	R^2	β (g/mg)	α (mg/g.mn)
4.45	0.795	1.4802	2.418
13.5	0.885	0.9525	12.493
17.6	0.787	1.1169	234.69

On the contrary, the determination coefficient and $q_{e,cal}$ of the pseudo-second order kinetic model agree with the experiments (Table 5).

Elovich equation (Gerente et al., 2007). Although the Elovich equation was firstly used in the kinetics of chemisorptions of gases on solid, it has been successfully applied for the adsorption of solutes from a liquid solution. The Elovich equation is given as follows

$$q_t = \frac{1}{\beta} \ln\alpha.\beta + \frac{1}{\beta}.\ln t \qquad (12)$$

where α (mg/g min) is the initial sorption rate, the parameter β (g/mg) is related to the extent of surface coverage and activation energy for the chemisorptions. The plot q_t versus ln t was used to determine the constants α and β.
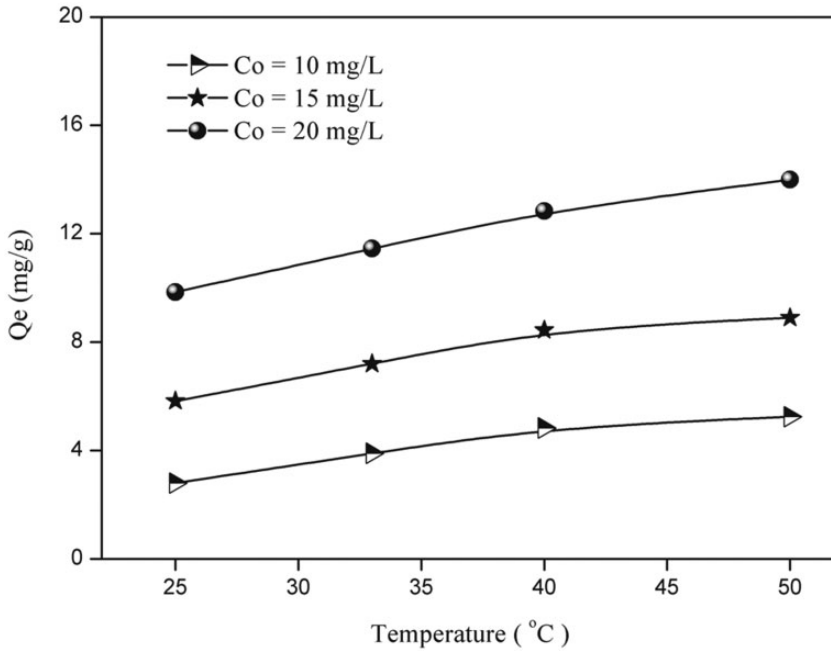
Effect of temperature

Figure 12 clearly shows that the adsorption capacity of ASM increases with increasing the MG concentration (10 to 20 mg/L) and temperature (295 to 323 K), indicating that the adsorption is favored at high temperature. The free energy ($\Delta G°$), enthalpy ($\Delta H°$), and entropy ($\Delta S°$) are determined by the following equations (Kin et al., 2005; Zahia et al., 2019b)

$$\Delta G° = \Delta H° - T\Delta S° \qquad (13)$$

The free energy is composed of the enthalpic term ($\Delta H°$) which expresses the energies of interactions molecules/adsorbent surface, and entropic term ($\Delta S°$) which expresses the modification and arrangement of the molecules in the liquid phase and on the surface.

The thermodynamic behavior for MG adsorption onto ASM was further investigated. The thermodynamic parameters $\Delta G°$, $\Delta H°$, and $\Delta S°$ are calculated from the relation

Figure 12. Temperature effect on the adsorption of MG onto ASM (C_o: 10 to 20 mg/L, pH: 10, adsorbent dosage: 1 g/L, particle size: 800–2000 µm, stirring speed: 400 r/min and contact time: 40 min).

$$\Delta G^{\circ} = -\mathrm{RT}\ln K_o \tag{14}$$

K_o is the apparent equilibrium constant. ΔH° and ΔS° are calculated from the adsorption data at different temperatures using the relation

$$\ln K_o = -\frac{\Delta H^{\circ}}{RT} + \frac{\Delta S^{\circ}}{R} \tag{15}$$

The values of ln K_o were obtained from equilibrium constant (K_s)

$$K_s = \frac{q_e}{C_e} \times \frac{\gamma_1}{\gamma_2} \tag{16}$$

where γ_1 is the activity coefficient of the adsorbed solute and γ_2 the activity coefficient of the solute in the equilibrium suspension. The ratio of activity coefficients was assumed to be uniform for dilute solutions. As the MG concentrations in solution approached zero, the activity coefficient approached unity

$$\lim_{C_e \to 0} \frac{q_e}{C_e} = K_0 \tag{17}$$

$Y = -6113.634\ x + 20.565$
$R^2 = 0.9999$
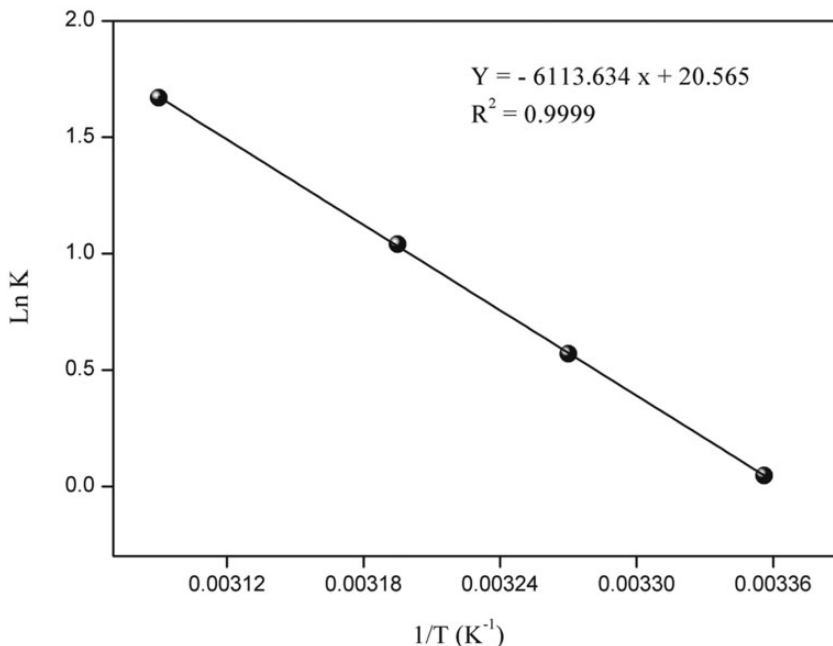
Figure 13. Thermodynamic parameters, enthalpy, and entropy for the adsorption of MG ions onto ASM.

Table 6. Thermodynamic parameters for the MG adsorption on ASM.

T (K)	$1/T$ (K^{-1})	K	ln K	$\Delta G°$ (kJ/mol)	$\Delta H°$ (kJ/mol)	$\Delta S°$ (J/mol.K)
298	0.00336	1.04	0.047	−0.191	50.86	171.09
306	0.00327	1.76	0.569	−1.539		
313	0.00319	2.83	1.04	−2.737		
323	0.00309	5.32	1.67	−4.447		

The values of K_0 determined from intercept (figures not shown), by plotting $\ln(q_e/C_e)$ versus C_e and extrapolating to $C_e = 0$ at different temperatures (Ghaedi et al., 2013). $\Delta H°$ and $\Delta S°$ obtained from the slope and intercept of the plot ln K versus $1/T$ (Figure 13) and $\Delta G°$ at various temperatures are summarized in Table 6. The negative free energy $\Delta G°$ (−0.191 to −4.447 kJ/mol) and positive enthalpy $\Delta H°$ (50.86 kJ/mol) indicate that the adsorption of MG onto ASM is spontaneous and endothermic. The positive entropy $\Delta S°$ (171 J/mol.K) states clearly that the randomness increases at the solid–solution interface during the MG adsorption, indicating that some structural exchange occurred among the active sites of the adsorbent and MG.

Performance of the prepared ASM

In order to evaluate the efficiency of ASM, a comparison of basic dye adsorption of this work is made with other relevant studies (Table 7) and the adsorption capacity (q_{max}) is the key comparative parameter. We can see that our q_{max} value is in good agreement with most

Table 7. Comparison of ASM's performances with precursors from previous studies.

Adsorbants	q_{max} (mg/g)	T (°C)	pH	t_{eq} (h)	References
Activated carbon	565	32	10	48	Kumar (2006)
Jute fiber carbon	136.6	25	10	6	Porkodi and Kumar (2007)
Biomass of phitophora	117.6	30	5	8	Kumar et al. (2005)
Activated carbon (waste apricot)	116.3	30	9	1	Basa (2006)
	158.73	40	8	1	
	163.93	50	8	1	
Cyclodextrin-based adsorbent	91.9	25	8	2	Crini et al. (2007)
Hen feathers	10.29	25	5	3	Mittal (2006)
	10.69	40	5	3	
	35.79	50	5	3	
Arundo Domax root carbon	8.49	20	5	3	Zhang et al. (2008)
	8.69	30	5	3	
	9.35	40	5	3	
Sugar cane dust	4.88	25	7.5	0.5	Khattri and Singh (1999)
	4.57	35	7.5	0.5	
	4.08	45	7.5	0.5	
Lemon peel	51.73	32	10	25	Kumar and Sivanesan (2007)
Caulerpa racemosavar cylindracea	19.88	25	6	1.5	Bekci et al. (2009)
	21.74	25	6	1.5	
	25.67	25	6	1.5	
Bamboo-based activated carbon	263.6	30	8	3.5	Hameed and El Khaiary (2008)
Commercial activated carbon	8.27	30	7	3	Mall et al. (2005)
Laboratory grade	42.18	30	7	3	
Bagasse fly ash	170	30	7	3	
Rubber wood sawdust	36.3	30	9	48	Kumar and Sivanesan (2007)
Functionalized sawdust	85.47	25	8	25	Renmin et al. (2009)
Crude sawdust	196.08	25	8	25	
Dead tree leaves	78.45	25	9	0.5	Oualid et al. (2008)
	83.21	35	9	0.5	
	86.21	45	9	0.5	
Apricot stone activated carbon (ASM)	23.94	25	10	40 min	This study
ASM	88.5	70	10	40 min	

previous works, suggesting that MG could be easily adsorbed on ASM prepared in the present work and the apricot stones, very abundant in Algeria, are effective adsorbent for the MG adsorption. ASM is a promising adsorbent for heavy metals and basic dyes owing to pHpzc, and our perspective in the future is to achieve the adsorption tests in column mode using industrial effluents. Such results are currently under way and will be reported in a next future.

Conclusion

This study has shown that the activated carbon prepared from apricot stone can be employed as effective adsorbent for the removal of MG in aqueous solution. The Langmuir model provided a better fit of the equilibrium adsorption data. It gave a maximum adsorption capacity of 23.80 mg/g at 25°C which increased down to 88.05 mg/g at 70°C at pH 10.

The pseudo second-order model proved the best description of the kinetic data. The negative free energy $\Delta G°$ and positive enthalpy $\Delta H°$ indicate that the adsorption of MG onto ASM is spontaneous and endothermic over the studied temperatures range. The positive entropy $\Delta S°$ states clearly that the randomness increases at the solid–solution interface during the MG adsorption onto ASM, indicating that some structural exchange occurred among the active sites of the adsorbent and MG ions.

The MG adsorption follows a pseudo second-order kinetic model, which relies on the assumption that the chemisorptions may be the rate-limiting step. The MG molecules are attached to the adsorbent surface by forming a chemical bond and tend to find sites that maximize their coordination number with the surface. The kinetic and thermodynamic data can be further explored for the design of absorber for industrial effluents treatment.

The results of the present investigation showed that ASM is a potentially useful adsorbent for the MG adsorption, an issue of environmental concern and the natural abundance of this food waste can provide an adsorption medium which contributes to the wastewater treatment. The comparison of the adsorption capacity of the prepared adsorbent with other adsorbents shows its attractive properties from industrial and economic interests.

This study in tiny batch gave rise to encouraging results, and we wish to achieve the adsorption tests in column mode under the real conditions applicable to the treatment of industrial effluents and to test the homogeneous photodegradation of MG on TiO_2 and SnO_2 semiconductors is the future objective of this work.

Declaration of Conflicting Interests

The author(s) declared no potential conflicts of interest with respect to the research, authorship, and/or publication of this article.

ORCID iD

Moussa Abbas ⓘ https://orcid.org/0000-0002-0420-2414

References

Abbas M, Aksil T and Trari M (2018) Removal of toxic Methyl Green (MG) in aqueous solution by apricot stone activated carbon – Equilibrium and isotherm modeling. *Desalination and water Treatment* V125: 9–101.

Abbas M, Cherfi A, Kaddour S and Aksil T. (2016) Adsorption in simple batch experiments of Coomassie Blue G-250 by apricot stone activated carbon-kinetics and isotherms modeling. *Desalination and Water Treatment* V57(32): 15037–15048.

Abbas M, Kaddour S and Trari M (2014) Kinetic and equilibrium studies of cobalt adsorption on apricot stone activated carbon. *Journal of Industrial and Engineering Chemistry* V20: 745–751.

Abbas M and Trari M (2015) Equilibrium and thermodynamic study on the removal of Congo Red from aqueous solutions by adsorption onto apricot stone. *Process Safety and Environment Protection* V98: 436–445.

Abbas M, Zahia H and Mohamed T (2019) Removal of Gentian Violet in aqueous solution by activated carbon equilibrium, kinetics, and thermodynamic study. *Adsorption Science & Technology* V37(7–8): 566–589.

Basa CA (2006) Applicability of the various adsorption models of three dyes adsorption onto activated carbon prepared waste apricot. *Journal of Hazardous Materials* B135: 232–241.

Bekci Z, Seki Y and Cavas L (2009) Removal of malachite green by using an invasive marine alga Caulerpa Nacemosa var. cylindracea. *Journal of Hazardous Materials* V161: 1454–1460.

Crini G, Peindy HN, Gimbert F, et al. (2007) Romoval of C.I. Basic green 4 (Malachite Green) from aqueous solutions by adsorption using cyclodextrin-based adsorbent: Kinetic and equilibrium studies. *Separation and Purification technology* V53: 97–110.

El-Sheikh AH, Newman AP, Al-Daffaee HK, et al. (2004) Characterization of activated carbon prepared from a single cultivar of Jordanian olive stones by chemical and physicochemical techniques. *Journal of Analytical and Applied Pyrolysis* V71: 151–164.

Food and Agriculture Organization of the United Nations (FAO) (2017) *Production Directory*. Rome: FAO.

Freundlich HMF (1906) Über die adsorption in lösungen. *Zeitschrift für Physikalische Chemie (Leipzig)* 57A: 385–470.

Gerente C, Lee VKC, Le CLoirec P, et al. (2007) Application of chitosan for the removal of metals from wastwater by adsorption – Mechanism and model review. *Critical Reviews in Environmental Science and Technology* V37: 41–127.

Ghaedi M, Karimi F, Barazesch B, et al. (2013) Removal of reactive Orange 12 from aqueous solutions by adsorption on tin sulfide nanoparticle loaded on activated carbon. *Journal of Industrial and Engineering Chemistry* V19(3): 756–763.

Giles CH, Mac Ewan TH, Nakhwa SN, et al. (1960) Studies in adsorption. Part XI. A system of classification of solution adsorption isotherms, and its use in diagnosis of adsorption mechanisms and in measurement of specific surface areas of solids. *Journal of the Chemical Society* V10: 3973–3993.

Hameed BH, Din ATM and Ahmad AL (2007) Adsorption of methylene blue onto bamboo-based activated carbon: Kinetics and equilibrium studies. *Journal of Hazardous Materials* V141: 819–825.

Hameed BH and El Khaiary MI (2008) Equilibrium, kinetics and mechanism of malachite green adsorption on activated carbon prepared from bamboo by K_2CO_3 activation and subsequent gasification with CO_2. *Journal of Hazardous Materials* V157: 344–351.

Ho YS and Mc Kay G (2000) The kinetics of sorption of divalent metal ions onto sphagnum moss peat. *Water Research* V34(3): 735–742.

Iqbal MJ and Ashiq MN. (2007) Adsorption of dyes from aqueous solutions onactivated charcoal. *Journal of Hazardous Materials* V139(1): 57–66. DOI: 10.1016/j.jhazmat.2006.06.007.

Isık M and Sponza DT (2005) A batch study for assessing the inhibition effect of Direct Yellow 12 in a mixed methonogenic culture. *Process Biochemistry* V40: 1053–1062.

Kannan N and Sundaram MM (2001) Kinetics and mechanism of removal of methylene blue by adsorption on various carbons – A comparative study. *Dyes and Pigments* V51: 25–40.

Khattri SD and Singh MK (1999) Colour removal from dye wastewater using sugar cane dust as an adsorbent. *Adsorption Science & Technology* V17: 269–282.

Kin T-Y, Park KS, Cho YS, et al. (2005) Adsorption of metals by brewery biomass. *Korean Journal of Chemical Engineering* V22(1): 91–98.

Kumar KV (2006) Comparative analysis of linear and non linear method of estimating the sorption isotherm parameters for Malachite Green onto activated carbon. *Journal of Hazardous Materials* B136: 197–202.

Kumar KV and Sivanesan S (2007) Isotherms for malachite green onto rubber wood (Hevea brasi-liensis) sawdust: Comparison of linear and non linear methods. *Dyes and pigments* V21(1): 124–129.

Kumar KV, Sivanesan S and Ramamurthy V (2005) Adsorption of malachite green onto Pithophora, fresh water algae: Equilibrium and kinetic modeling. *Process Biochemistry* V40: 2865–2875.

Lagergren S (1998) About the theory of so-called adsorption of soluble substances. *K Sven Ventensskapsakad Handlingar Band* V24: 1–39.

Leigen L, Zhenfeng L, Jiantao N, et al. (2019) Electrospun polysulfone/poly (lactic acid) nanoporous fibrous mats for oil removal from water. *Adsorption Science & Technology* V37(5–6): 438–450.

Limousin G, Gaudet J-P, Charlet L, et al. (2007) Sorption isotherms: A review on physical bases, modeling and measurement. *Applied Geochemistry* V22: 249–275.

Malik R, Ramteke DS and Wate SR (2007) Adsorption of Malachite Green on groundnut shell waste based powdered activated carbon. *Waste Management* V27(9): 1129–1138.

Mall ID, Srivastava VC, Agarwal NK, et al. (2005) Adsorptive removal of Malachite Green dye from aqueous solution by bagasse fly ash and activated carbon, kinetic study and equilibrium isotherm analyses. *Colloids and Surfaces A: Physicochemical and Engineering Aspects* 264: 17–28.

Mittal A (2006) Adsorption kinetics of removal of toxic dye, Malachite Green from wastewater by using hen feathers. *Journal of Hazardous Materials* B133: 196–233.

Namasivayam C and Kavitha D (2002) Removal of Congo Red from water by adsorption onto activated carbon prepared from coir pith, an agricultural solid waste. *Dyes and Pigments* 54: 47–58.

Oualid H, Fethi S, Mahdi C, et al. (2008) Sorption of Malachite Green by novel sorbent, dead leaves of plane tree: Equilibrium and kinetic modeling. *Chemical Engineering Journal* V143(1–3): 73–84.

Ozcan A, Oncu EM and Ozcan AS (2006) Kinetics, isotherm and thermodynamic studies of adsorp-tion of Acid Blue 193 from aqueous solutions onto natural sepiolite. *Colloids and Surfaces A: Physicochemical and Engineering Aspects* V277(1–3): 90–97.

Porkodi K and Kumar KV (2007) Equilibrium, kinetics mechanism modeling and simulation of basic and acid dyes sorption onto jute fiber carbon: Eosin yellow, malachite green and crystal violet single component systems. *Journal of Hazardous Materials* V143: 311–327.

Qi-Xia L, Yi-Ru Z, Mei W, et al. (2019) Adsorption of Methylene Blue from aqueous solution onto viscose-based activated carbon fiber felts: Kinetics and equilibrium studies. *Adsorption Science § Technology* V37(3–4): 312–232.

Rengaraj S, Moon SH, Sivabalan R, Arabindoo B and Murugesan V (2002) Removal of phenol from aqueous solution and resin manufacturing industry wastewater using an agricultural waste: rubber seed coat. *Journal of Hazardous Materials* 89(2-3): 185–196. DOI: 10.1016/S0304-3894(01)00308-9.

Renmin G, Min F, Jiajing Z, et al. (2009) Functionalization of sawdust with monosodium glutamate for enhancing its malachite green removal capacity. *Bioresource Technology* V100(2): 975–978.

Temkin M.I and Pyzhev V (1940) Recent modifications to Langmuir isotherms. *Acta Physicochimca URSS* 12: 327–356.

Zahia H, Moussa A, Tounsia A, et al. (2019a) Thermodynamic and kinetics studies on adsorption of Indigo Carmine from aqueous solution by activated carbon. *Microchemical Journal* V144: 180–189.

Zahia H, Moussa A, Tounsia A, et al. (2019b) Modeling of adsorption isotherms of (5, 5′-disodium indigo sulfonate) from aqueous solution onto activated carbon: Equilibrium, thermodynamic stud-ies, and error analysis. *Desalination and Water Treatment* V147: 273–283.

Zhang J, Yan Li Zhang C and Jing Y (2008) Adsorption of Malachite Green from aqueous solution onto carbon prepared from Arundo donax root. *Journal of Hazardous Materials* V150: 774–782.